

## COUPLING A BOUNDARY LAYER WALL SHEAR-STRESS MODEL WITH FIELD EXPERIMENTS IN A SHALLOW TIDAL RIVER

**Romain Mathis**

Laboratoire de Mécanique de Lille  
 CNRS UMR 8107, Université Lille Nord de France  
 59655 Villeneuve d'Ascq, France  
 romain.mathis@univ-lille1.fr

**Ivan Marusic**

Department of Mechanical Engineering  
 University of Melbourne  
 Victoria, 3010 Australia  
 imarusic@unimelb.edu.au

**Nicole L. Jones & Gregory N. Ivey**

School of Environmental Systems Engineering and UWA Oceans Institute  
 University of Western Australia  
 Crawley, Western Australia, Australia  
 nicole.jones@uwa.edu.au, greg.ivey@uwa.edu.au

### ABSTRACT

Recently, Mathis *et al.* (2011) developed a conceptual approach that is able to predict instantaneous wall-shear stress fluctuations in turbulent boundary layers. This approach embeds the scale interaction mechanisms, namely superposition and modulation, into a wall-model capable of predicting the fluctuating component of the streamwise wall-shear stress. The present study investigates the potential benefits of this new approach for research on environmental flows, where near-wall information is often missing. The database considered here comes from field measurements using acoustic Doppler velocimeters carried out in a shallow tidal river (Suisun Slough in North San Francisco Bay). Amongst the data, only the sets having defined boundary layer properties are retained. The model, applied to these selected cases, shows promising results. Despite significant uncertainties in the field measurements, statistical analysis and comparisons of energy content demonstrate that predictions using these data agree relatively well with laboratory predictions and DNS results.

### INTRODUCTION

In wall-bounded turbulent flows the wall shear-stress  $\tau_w$  constitutes a key parameter for accurate prediction of the flow behaviour. Over the years, many studies have been devoted toward understanding and modelling the Reynolds number dependency of the mean, time-averaged, value  $\bar{\tau}_w$ , which is used in boundary layer inner-scaling via the friction velocity  $U_\tau = \sqrt{\bar{\tau}_w/\rho}$ , where  $\rho$  is the fluid density (see for example Schlichting & Gersten, 2000; Monkewitz *et al.*, 2007, amongst others). However, little is known about the fluctuating component,  $\tau'_w$ , which can be responsible for extreme and destructive events, such as wind gusts in atmospheric flows or scouring and mechanical damage on an aircraft (see figure 3 of Örlü & Schlatter, 2011). In environmental flows, the wall shear-stress is of great ecological importance where it is linked to erosion, bed formation, sediment and nutrient transportation, etc (Grant & Madsen, 1986; Rowiński *et al.*, 2005; Grant & Marusic,

2012). Unfortunately, the wall shear-stress is largely inaccessible in field measurements, which prompts the need for predictive models to reconstruct the missing information. Here, the fluctuating component is defined as  $\tau'_w(\mathbf{x}, t) = \tau_w(\mathbf{x}, t) - \bar{\tau}_w(\mathbf{x})$ , where  $\tau_w(\mathbf{x}, t)$  and  $\bar{\tau}_w(\mathbf{x})$  are the total and mean values of the wall shear-stress, respectively. The coordinates  $x$ ,  $y$  and  $z$  refer to the streamwise, spanwise and wall-normal directions. The respective fluctuating velocity components are denoted by  $u$ ,  $v$  and  $w$ . Over-bars indicate time-averaged values, and the superscript “+” is used to denote viscous scaling of length  $z^+ = zU_\tau/\nu$  and velocities  $u^+ = u/U_\tau$ , where  $\nu$  is the kinematic viscosity of the fluid.

Recently, Mathis *et al.* (2013) proposed a novel conceptual approach to build up a predictive model able to reconstruct the fluctuating wall shear-stress based on a single point measurement taken in the log-layer away from the wall. The model is based on many years of empirical observations, both experimental and numerical, that have clearly established that strong interactions exist between the near-wall region and motions in the outer region. Namely, the Reynolds number effects are closely related to the increasingly energetic content of the large-scale structures associated with the log-layer (Kim & Adrian, 1999; del Álamo & Jiménez, 2003; Hutchins & Marusic, 2007a, amongst others), through superposition and modulation effects (Bandyopadhyay & Hussain, 1984; Grinvald & Nikora, 1988; Hutchins & Marusic, 2007b; Mathis *et al.*, 2009, 2011). The wall-shear stress model was originally derived from the streamwise velocity model developed by Marusic *et al.* (2010) and Mathis *et al.* (2011), where an algebraic relationship between the streamwise velocity component and the wall shear stress is known, and is of the form:

$$\tau'_{wp}(t^+) = \tau_w^{*+}(t^+) \{1 + \alpha u_{OL}^+(t^+)\} + \alpha u_{OL}^+(t^+), \quad (1)$$

where  $\tau'_{wp}$  is the predicted time-series normalised by wall variables,  $\tau'_{wp} = \tau'_w/(\rho U_\tau^2)$  and  $t^+ = tU_\tau^2/\nu$ . The time-series  $\tau_w^{*+}$ , which is normalised in wall units, represents the

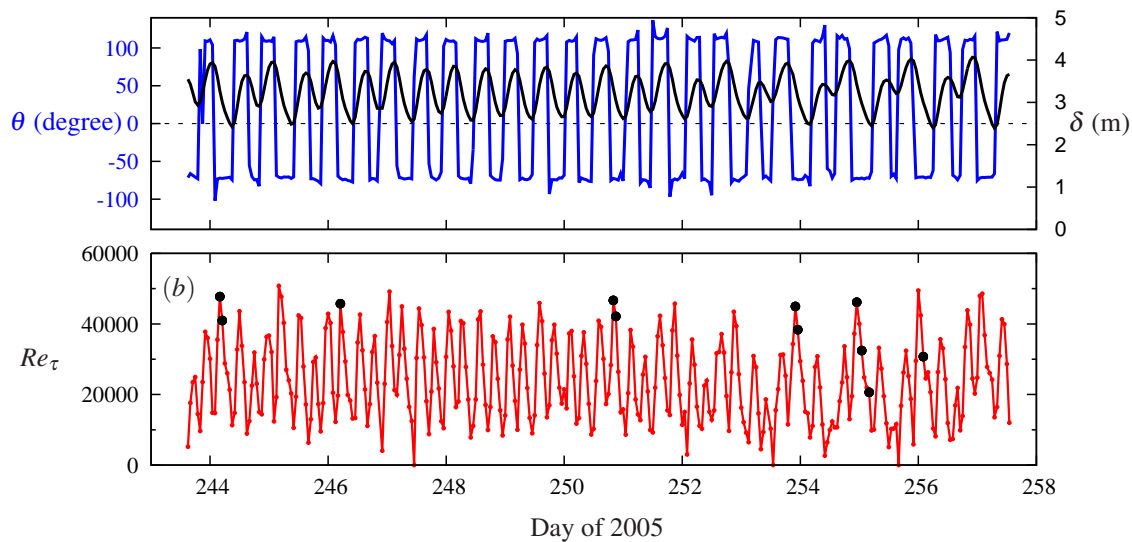


Figure 1. (a) Mean flow direction  $\theta$  (blue), and depth of water (black) used as boundary layer thickness  $\delta$ ; (b) Reynolds number of each burst (black dots denote the selected cases).

statistically “universal” wall shear-stress signal that would exist in the absence of any inner-outer interactions. The parameters  $\tau_w^*$  and  $\alpha$  are determined from a once-off calibration experiment at an arbitrarily chosen Reynolds number, and are hypothesized to be Reynolds number independent. The only user input required for the model is a characteristic signal of the large-scales from the log-region,  $u_{OL}^+$ , taken nominally at the geometric centre of the log-layer,  $z_O^+ = \sqrt{15Re_\tau}$ , where  $Re_\tau = U_\tau \delta / \nu$  is the friction Reynolds number and  $\delta$  the boundary layer thickness (see Mathis *et al.*, 2009, 2011, for further details about the choice of  $z_O^+$ ). The model consists of two parts. The first part in equation 1 models the amplitude modulation of the small-scales, here  $\tau_w^*$ , by the large-scale log-region motions,  $u_{OL}^+$ . The second term,  $\alpha u_{OL}^+$ , models the superposition of the large-scale motions felt at the wall. The underlying idea is that the near-wall small-scale motions are universal (i.e. they do not change with Reynolds number), and therefore are only influenced by large-scale log-region events (the intensity of the influence increasing with increasing Reynolds number). Therefore, the Reynolds number effects are confined to the large-scale log-region input signal,  $u_{OL}^+$ .

The purpose of the present study is to verify whether this approach is suitable to environmental flows, where effects such as roughness or stratification may be important. The model was initially developed and calibrated for the flat-plate smooth-wall turbulent boundary layer, and therefore its applicability in environmental flows is not straightforward. As such, a tidal river dataset is used to predict what is happening at the bed. Results, including statistical properties and spectral content, are analysed and compared with flat-plate smooth-wall turbulent boundary layer data from the literature, as well as with previous predictions using laboratory measurements.

## EXPERIMENTAL DATASET

The dataset used here comes from field experiments of Jones *et al.* (2009) carried out in Suisun Slough in North San Francisco Bay from 30 August to 15 September 2005. The section of Suisun Slough where the measurements were undertaken is relatively shallow, with the water-depth rang-

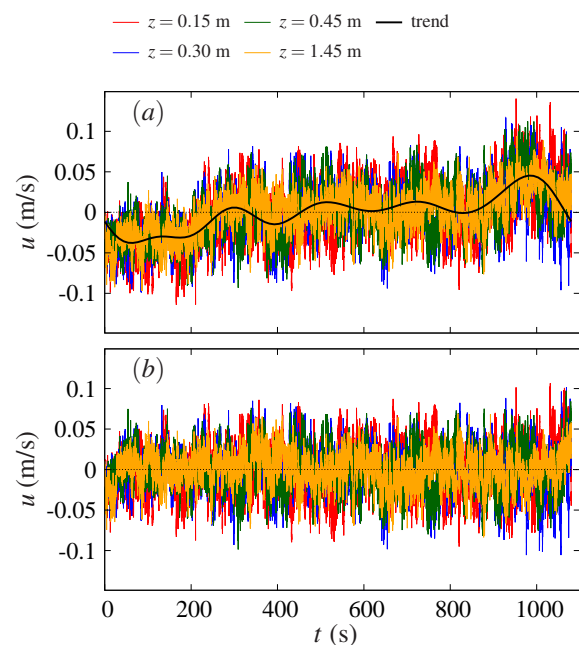


Figure 2. Fluctuating streamwise velocity at each height, (a) before and (b) after detrend. The black solid line in (a) corresponds to the trend calculated by low-pass filtering the average of the 4 heights. Selected case corresponds to the burst 70, day  $\sim 246.5$ .

ing from 2.5 to 4.0 m with the semidiurnal tide. Measurements of the three velocity components were made using acoustic Doppler velocimeters (ADV, Nortek AS), at four different heights (0.15, 0.3, 0.45 and 1.45 m). The dataset consists of 330 bursts, sampling for 20 minutes of every half hour at 16 Hz. A full description of the experiment and measurement procedure is available in Jones *et al.* (2009). The site’s hydrodynamics are dominated by tidal flow, producing a cyclic change in the mean flow direction and depth of water (Fig. 1(a)). This leads to a large range of Reynolds numbers as seen in figure 1(b).

Each burst of measurements, initially acquired in

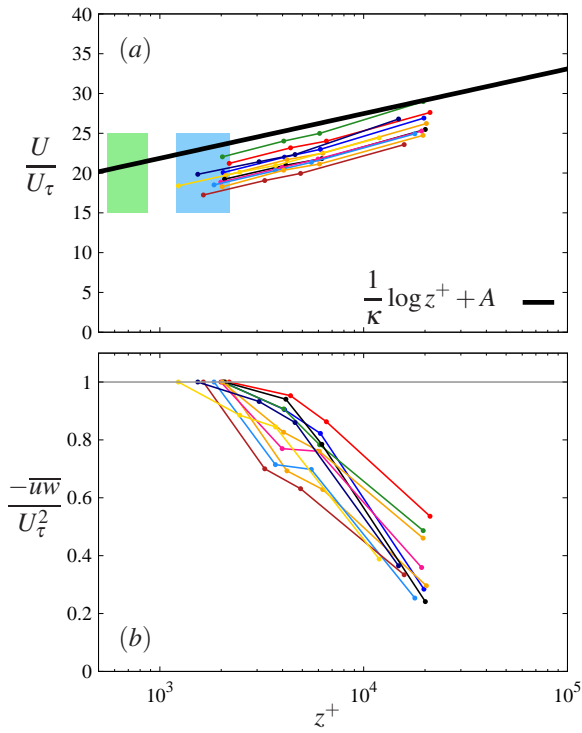


Figure 3. (a) Mean velocity, and (b) Reynolds shear-stress profiles of the selected cases.

North, East and Up/down coordinates, are first transposed to a right-handed coordinate system in which the stream-wise direction corresponds to the mean flow direction. This is done by determining a mean flow angle for each burst of 20 minutes. Samples of the turbulent fluctuations, given in figure 2(a) for the streamwise component, show that a long-term trend emerges from the signal. This trend corresponds to the natural variability of the river environment, and has a wavelength much longer than the largest-scale motion observed in a turbulent boundary layer, typically of length  $10\delta - 15\delta$  (equivalent to 100-150s in the present data). As we will use the large-scale turbulent component of the signal to reconstruct the bed information, it is necessary to separate these effects by applying a filtering process. The velocity signals from the four wall-normal locations are averaged together (for each burst), then low-pass filtered at a cut-off wavelength of  $20\delta$  (equivalent to about 200s). The resulting long-term trend is then subtracted from the velocity signal (Fig. 2(b)). Once this is done, the mean friction velocity  $U_\tau$  can be estimated using the Reynolds stress peak, i.e.,  $U_\tau = \max(\sqrt{-\overline{uw}}(z))$ . It should be emphasised that this estimation is somewhat inaccurate, particularly due to the limited range and number of points in the wall-normal direction (see figure 3(b)).

The primary goal of this study is to assess the potential for the wall-shear stress model of Mathis *et al.* (2013) to be applied to environmental flows, particularly as the model was originally developed for a smooth-wall zero-pressure-gradient turbulent boundary layer. It is acknowledged that the model's parameters claimed to be "universal" by Mathis *et al.* (2013) in the case of the smooth-wall zero-pressure-gradient turbulent boundary layer, might not be fully adequate for the present flow conditions. However, even if variability of these "universal parameters" might exist between different types of wall-bounded flows (e.g. affected by pressure-gradient, roughness, secondary flows,

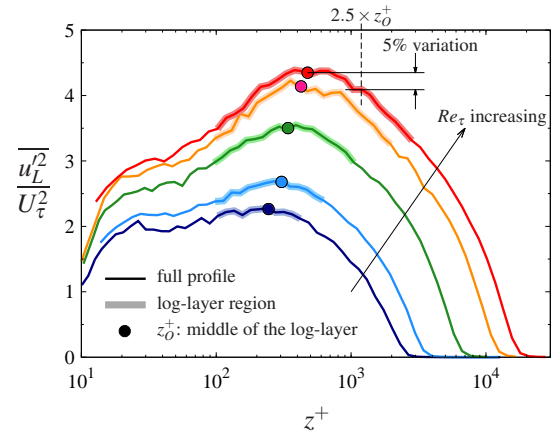


Figure 4. Wall-normal evolution of the large-scale streamwise turbulent intensity  $\overline{u_L'^2}$  (filter cutoff set to  $\lambda_{c,x} = 7000$ ), for laboratory measurements  $2800 \leq Re_\tau \leq 19000$  (Hutchins *et al.*, 2009; Mathis *et al.*, 2009); For the highest Reynolds number 5% variation of the peak intensity occurs at  $z^+ = 2.5 \times z_O^+$ .

etc), this should affect only the accuracy of the model, and not the overall Reynolds number trends (Mathis *et al.*, 2011). Therefore, in this first approach a selection of bursts are considered, aiming to retain only cases that have statistics close to the canonical turbulent boundary layer. A first selection is made by discarding bursts in which the mean velocity profile does not fit within  $\pm 10\%$  of the classical log-law behaviour  $\overline{u^+} = \frac{1}{\kappa} \log z^+ + A$ , with  $\kappa = 0.41$  and  $A = 5.0$  (see figure 3(a)). It should be noted that only the first three wall-normal locations are situated within the logarithmic layer, and thus only these are used for the log-fit (assuming the log-region applied for  $100 < z^+ < 0.15Re_\tau$ ). The mean velocity profiles were consistently below the log-law, likely due to bed roughness (Fig. 3(a)). Finally, we have only used data that has a Reynolds stress  $-\overline{uw}$  profile that monotonically decays towards the top of the boundary layer (Fig. 3(b)). This selection method yields 11 usable cases amongst the 330 original bursts, covering a range of Reynolds numbers from  $Re_\tau \simeq 20,000$  to 50,000.

## INPUT LARGE-SCALE OUTER SIGNAL

The predictive wall shear-stress model, developed by Mathis *et al.* (2013), requires as input large-scale information. Ideally, this input signal should be from the middle of the log-layer,  $z_O^+ = \sqrt{15Re_\tau}$ , corresponding to the outer-spectral-peak location (see figure 12 in Mathis *et al.*, 2009) where the large-scales have the most energetic signature, as seen in figure 4. As shown by Cabrit *et al.* (2012), variations in the predicted wall-shear stress might occur if the location of the input large-scale information deviates excessively from the middle of the log-layer. Indeed, as seen in figure 4, any variation from the optimal wall-normal location induces a reduction in the energy of the input signal of the model and hence the predictions are under-estimated (Cabrit *et al.*, 2012). As the Reynolds number increases, the sensitivity to the wall-normal location is more acute as the peak in figure 4 becomes sharper. The optimal wall-normal location is not always easily accessible in environmental flows, particularly as  $U_\tau$ , and  $Re_\tau$  are also subject to variation. Therefore, data are usually collected at a fixed physical wall-normal location. In the present dataset, the lowest measurement point ( $z = 0.15$  m)

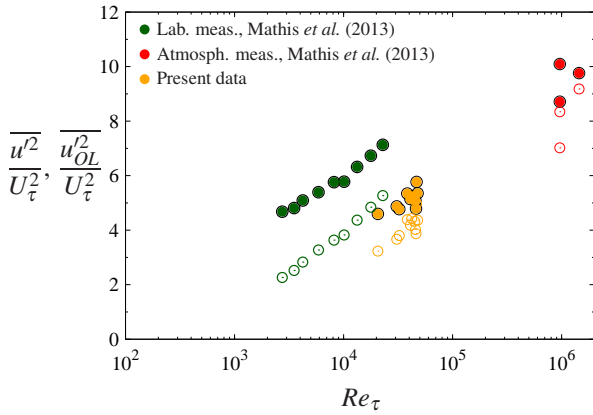


Figure 5. Reynolds number dependency of the streamwise turbulence intensity of the log-region unfiltered signal  $u_O^+$  (filled symbols), and the filtered large-scale component  $u_{OL}^{\prime+}$  (opened symbols).

is located 2.2 – 2.5 times above the optimal wall-normal location  $z_O^+ = \sqrt{15Re_\tau}$ . The green and blue shaded areas in figure 3(a) represent the extent of the location of the optimal and first measured points, respectively, for the range of Reynolds numbers  $20,000 \leq Re_\tau \leq 50,000$ . As seen in figure 4, for the highest Reynolds number, the intensity variation at  $z^+ = 2.5 \times z_O^+$  is about 5%. Therefore, we used the first wall-normal location to calculate the wall-shear stress.

The first wall-normal location ( $z_1 = 0.15$  m, i.e.  $z_1^+ \sim 2.2 - 2.5 \times z_O^+$ ) is used to form the input signal necessary for the model,  $u_{OL}^{\prime+}$ . The acquired raw signal at  $z_1^+$ , is first high-pass filtered at the non-dimensional frequency  $f^+ < 2.65 \times 10^{-3}$  to retain only the large-scale component. Then, the filtered signal is shifted forward in the streamwise direction to account for the large-scales structure angle (see Mathis *et al.*, 2013, for full details about how to calculate  $u_{OL}^{\prime+}$ ). The Reynolds number trend of the energetic content of the raw and filtered signal for each retained case are shown in figure 5, along with the laboratory and atmospheric measurements. Overall, both the unfiltered and filtered signals appear to have less energy than the smooth wall results, but they do follow the same Reynolds number trend. It is speculated that the lower intensity of the tidal river measurements, about 35% lower than laboratory measurements, is not directly related to the aforementioned miss-matched optimal wall-normal location (expected to be around 5%). Figure 6 shows the spectral content of the outer boundary layer signals for the present dataset and for the laboratory experiment for a similar Reynolds number. The discrepancy between the laboratory and field measurements may be attributable to measurement uncertainties, as the length of each burst is somewhat short for convergence of the large-scale content (18 minute sample corresponding to  $TU_\infty/\delta \approx 100$ ). This is clearly visible in figure 6 where the largest-scales of the field measurements are not resolved. However, it should be noted that the discrepancy observed between the laboratory and environmental experiments, might also be due to bed roughness effects and other phenomenon related to the dynamics of the tidal river. Also, there is no certainty that the large-scale structures exhibit the same properties in environmental flows, compared to the canonical laboratory configuration.

Even though the field measurements appear to slightly differ from laboratory measurements, they do retain the main characteristics of a wall-bounded flow. In the next sec-

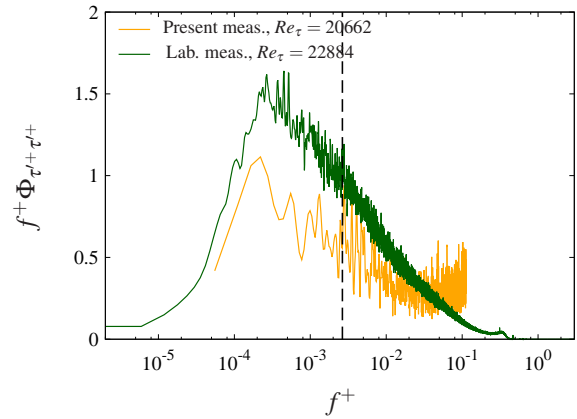


Figure 6. Pre-multiplied energy spectra of the input streamwise velocity signals for the laboratory and present measurements; The vertical dashed line shows the location of the cut-off frequency  $f^+ = 2.65 \times 10^{-3}$ .

tion we apply the wall-shear stress model in order to assess its potential and relevance for field measurements.

## PREDICTION

Now that  $u_{OL}^{\prime+}$  has been estimated, the wall-shear stress  $\tau_{wp}^+$  can be reconstructed using equation 1. Figure 7(a) shows the fluctuating intensity of the reconstructed wall shear-stress signal. Overall, the results agree relatively well with available DNS data and previous predictions made using laboratory measurements: the Reynolds number trend appears to be correctly captured, but a slight underestimation is observed. This is directly related to the aforementioned lower energy content of the input large-scale signal. The energy content of the reconstructed wall-shear stress signals is given in figure 8 for predictions made at  $Re_\tau \sim 20000$ , from laboratory and field measurements along with the universal small-scale energy spectra. Overall, both predictions are very similar and the large-scale content is well captured. Higher order statistics, skewness and kurtosis, are depicted in figures 7(b) and 7(c), respectively. Again, the results seem to agree relatively well with other predictions, even though significant scatter is present, most likely due to the short length of each burst leading to inadequate convergence of the large-scale statistics. Here,  $TU_\infty/\delta \approx 110$ , whereas it has been previously suggested that this number need to be large ( $> 5000$ ) to converge the large-scale content (Hutchins *et al.*, 2009). It should be noted that the skewness and kurtosis factors of the reconstructed wall-shear stress signal increase with Reynolds number at a lower rate than the low Reynolds number DNS. This is consistent with previous findings and is the subject of ongoing study.

Samples of the reconstructed instantaneous wall-shear stress signal, along with the input outer large-scale signal, are depicted in figure 9, for the lowest and highest predicted Reynolds numbers. It is interesting to note long and intense parts of positive and negative excursions, characteristic of very long large-scale motions (eventually up to  $20\delta$ ) developing within the log-region (Hutchins & Marusic, 2007a). The amplitude modulation of the wall-shear stress is also clearly visible at such high Reynolds numbers, i.e. attenuation and amplification appear respectively for negative and positive large-scale excursions (Hutchins & Marusic, 2007b; Mathis *et al.*, 2009). The highly skewed character

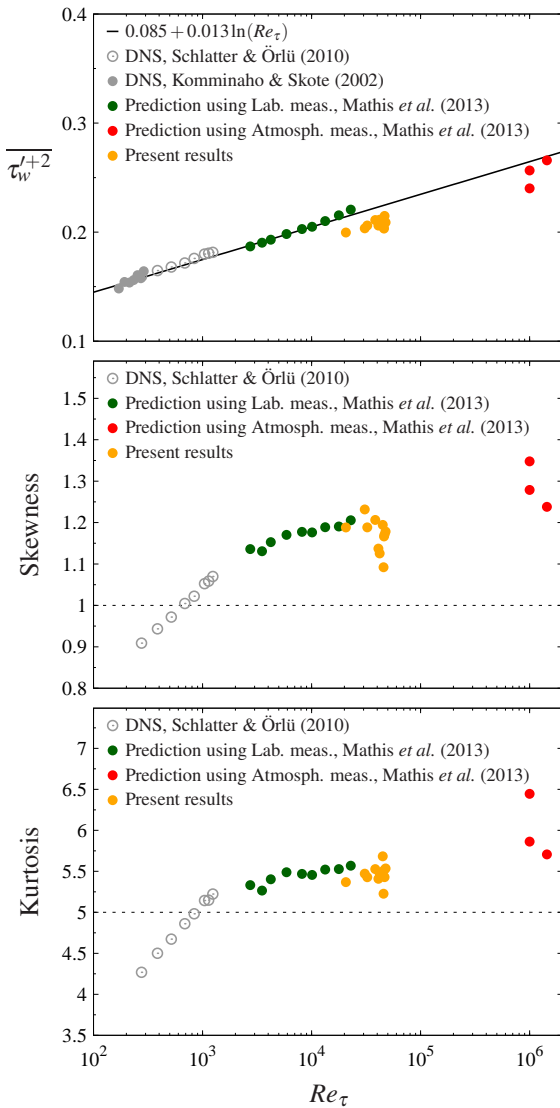


Figure 7. Fluctuation magnitude  $\overline{\tau_w'^2}$ , Skewness and Kurtosis of the predicted wall shear stress signal versus Reynolds number  $Re_\tau$ , compared to available data for DNS zero-pressure gradient turbulent boundary layer and former predictions using laboratory measurements.

of the wall-shear stress signal is also obvious.

## CONCLUSION

This paper discusses the potential benefits of the wall-shear stress model, developed by Mathis *et al.* (2011), applied to environmental flows. Here, a shallow tidal river is considered. Results show that the lack of near-wall information in such conditions can be partially reconstructed using the predictive model. Tests are performed here on a selection of dataset for which the properties are similar to the turbulent boundary layer. A closer analysis of the outer boundary layer signal resulting from these field measurements reveals strong similarity with laboratory measurements. The predictions based on these selected cases show a reasonable agreement with the trends of the laboratory and DNS results. While these preliminary results are encouraging, clearly further work is needed to fully develop the approach to general environmental flows. A generalised approach will need to account for additional effects, including

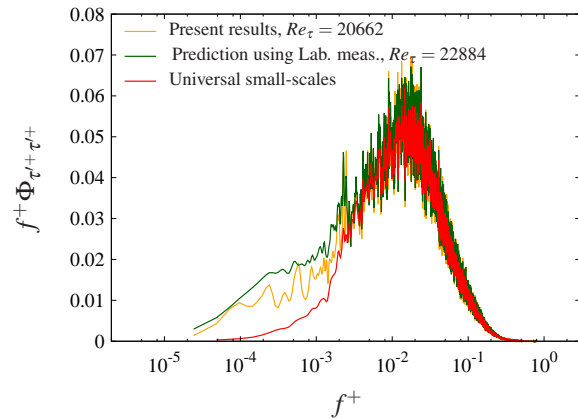


Figure 8. Pre-multiplied energy spectra of the predicted wall-shear-stress signal.

those of roughness, vegetation and stratification. It should also be emphasised that the dynamic nature of the tidal environment remains difficult to deal with. For example, it is difficult to obtain resolved large-scale information as any sample longer than the 18 minutes sampling time of the present dataset will be probably far from stationary in a tidal system.

## REFERENCES

- del Álamo, J. C. & Jiménez, J. 2003 Spectra of the very large anisotropic scales in turbulent channels. *Phys. Fluids* **15** (6), L41–L44.
- Bandyopadhyay, P. R. & Hussain, A. K. M. F. 1984 The coupling between scales in shear flows. *Phys. Fluids* **27** (9), 2221–2228.
- Cabrit, O., Mathis, R. & Marusic, I. 2012 Towards a statistically accurate wall-model for large-eddy simulation. In *18th Australasian Fluid Mechanics Conference*. Launceston, Australia.
- Grant, S. B. & Marusic, I. 2012 Crossing turbulent boundaries: Interfacial flux in environmental flows. *Environ. Sci. Technol.* **45**, 1443–1453.
- Grant, W. D. & Madsen, O. S. 1986 The continental-shelf bottom boundary layer. *Annu. Rev. Fluid Mech.* **18**, 265–305.
- Grinvald, D. & Nikora, V. 1988 *Rechnaya turbulentsiya (River Turbulence)*. Hydrometeoizdat, Russia, (in Russian).
- Hutchins, N. & Marusic, I. 2007a Evidence of very long meandering features in the logarithmic region of turbulent boundary layers. *J. Fluid Mech.* **579**, 1–28.
- Hutchins, N. & Marusic, I. 2007b Large-scale influences in near-wall turbulence. *Phil. Trans. R. Soc. Lond. A* **365**, 647–664.
- Hutchins, N., Nickels, T., Marusic, I. & Chong, M. S. 2009 Spatial resolution issues in hot-wire anemometry. *J. Fluid Mech.* **635**, 103–136.
- Jones, N. L., Thompson, J. K., Arrigo, K. R. & Monismith, S. T. 2009 Hydrodynamic control of phytoplankton loss to the benthos in an estuarine environment. *Limnol. Oceanogr.* **54** (3), 952–969.
- Kim, K. C. & Adrian, R. J. 1999 Very large-scale motion in the outer layer. *Phys. Fluids* **11**, 417–422.
- Komminaho, J. & Skote, M. 2002 Reynolds stress budgets in Couette and boundary layer flows. *Flow Turbul. and Combust.* **68**, 167–192.

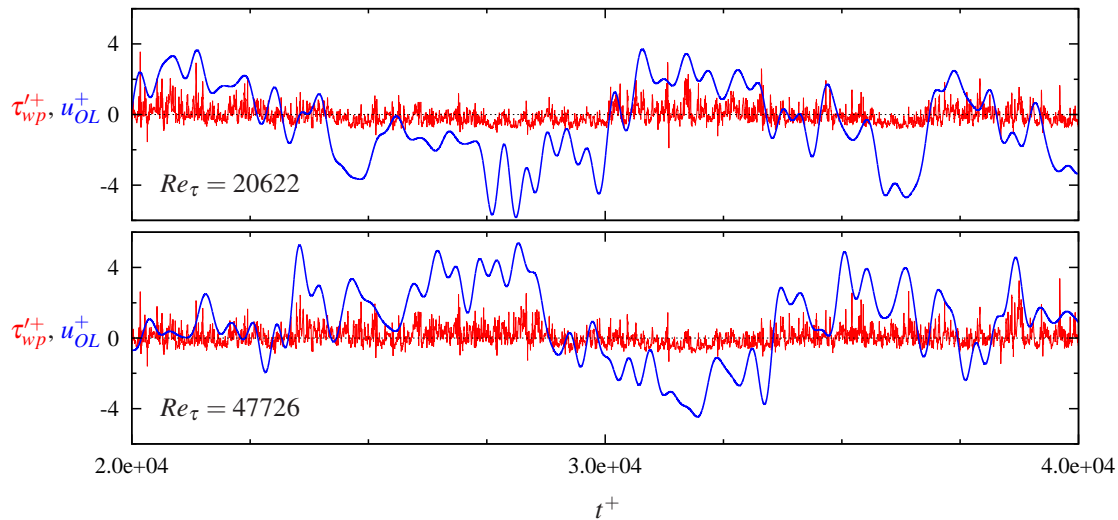


Figure 9. Samples of the predicted instantaneous wall-shear stress signal  $\tau_{wp}^+$ , with the input large-scale signal  $u_{OL}^+$  from the log-layer.

Marusic, I., Mathis, R. & Hutchins, N. 2010 Predictive model for wall-bounded turbulent flow. *Science* **329** (5988), 193–196.

Mathis, R., Hutchins, N. & Marusic, I. 2009 Large-scale amplitude modulation of the small-scale structures in turbulent boundary layers. *J. Fluid Mech.* **628**, 311–337.

Mathis, R., Hutchins, N. & Marusic, I. 2011 A predictive inner-outer model for streamwise turbulence statistics in wall-bounded flows. *J. Fluid Mech.* **681**, 537–566.

Mathis, R., Marusic, I., Chernyshenko, S. I. & Hutchins, N. 2013 A wall shear-stress predictive model for wall turbulence. *J. Fluid Mech.* **715**, 163–180.

Monkewitz, P. A., Chauhan, K. A. & Nagib, H. M. 2007 Self-consistent high-Reynolds-number asymptotics for

zero-pressure-gradient turbulent boundary layers. *Phys. Fluids* **19**, 115101.

Örlü, R. & Schlatter, P. 2011 On the fluctuating wall-shear stress in zero-pressure-gradient turbulent boundary layers. *Phys. Fluids* **23**, 021704, 1–4.

Rowiński, P., Aberle, J. & Mazurczyk, A. 2005 Shear velocity estimation in hydraulic research. *Acta Geophys. Pol.* **53** (4), 567–583.

Schlatter, P. & Örlü, R. 2010 Assessment of direct numerical simulation data of turbulent boundary layer. *J. Fluid Mech.* **659**, 116–126.

Schlichting, H & Gersten, K 2000 *Boundary layer theory*, eighth revised and enlarged edition edn. Springer.